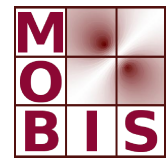
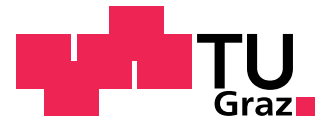




SpezialForschungsBereich F 32



Karl-Franzens Universität Graz  
Technische Universität Graz  
Medizinische Universität Graz



# Optimized Sampling Patterns for Random 3D Subsampling and Parallel Imaging Reconstruction by Regularized Nonlinear Inversion

Florian Knoll      Christian Clason  
Clemens Diwoky      Rudolf Stollberger

SFB-Report No. 2009-021

May 2009

A-8010 GRAZ, HEINRICHSTRASSE 36, AUSTRIA

Supported by the  
Austrian Science Fund (FWF)

**FWF** Der Wissenschaftsfonds.

SFB sponsors:

- **Austrian Science Fund (FWF)**
- **University of Graz**
- **Graz University of Technology**
- **Medical University of Graz**
- **Government of Styria**
- **City of Graz**



# Optimized 3D Random Sampling Patterns for Nonlinear Parallel Imaging Reconstruction

Florian Knoll\*, Christian Clason, Clemens Diwoky and Rudolf Stollberger

**Abstract**—A method is presented for scan time reduction in magnetic resonance imaging by combining an optimized random sampling pattern with a nonlinear reconstruction by iterative regularized Gauß-Newton. The sampling pattern is generated using a probability density function derived from the power spectrum of a reference image, which can be either taken from a pre-scan or a template. The proposed method allows artifact-free reconstruction of high resolution data sets even for high acceleration factors, and is shown to be robust, in particular with respect to the choice of reference images. This is confirmed by downsampling experiments as well as phantom and in vivo experiments.

**Index Terms**—MRI, Parallel Imaging, Random Sampling, IRGN.

## I. INTRODUCTION

**M**ANY important clinical applications of MRI like time resolved MR angiography or cardiac- and perfusion imaging require high resolution data sets in the spatial and temporal domain. It is still a challenging task to obtain these data sets in daily clinical practice, even with the use of ultra fast pulse sequences. This means that there is always a trade-off between temporal and spatial resolution. While data acquisition can be accelerated significantly by subsampling  $k$ -space, this leads to artifacts in the reconstructed images as the Nyquist sampling criterion is violated. Different strategies have been proposed to address this issue, such as parallel imaging [1], [2] or methods (usually summarized under the framework of compressed sensing [3], [4]) that exploit sparsity in certain transform domains. It has been shown recently that the reconstruction performance of Cartesian parallel imaging can be increased significantly by using a regularized nonlinear inversion method to jointly estimate coil sensitivities and image content [5]. It was also shown that this approach can be extended to radial imaging [6]. This enables the use of even higher acceleration factors, because the central frequencies of  $k$ -space, which define image contrast and are needed for

estimation of the coil sensitivities from the  $k$ -space data, are sampled more efficiently. However, even with non-Cartesian imaging, the ratio of high to low sampled frequencies is usually an arbitrary choice, and therefore not optimal.

Within the framework of compressed sensing, Lustig et al. [3] proposed the idea of randomized 3D Cartesian subsampling. These randomized sampling patterns can be generated by using Monte-Carlo simulations. With this approach, a probability density function (pdf) is constructed, and sampling pattern indices are drawn randomly from that density. This leaves the problem of designing a pdf that will generate an "optimal" sampling pattern, especially concerning the ratio of low- and high frequency sample points.

Variable density sampling patterns have already been studied in the past [7], [8], [9]. The goal of this work is to show that it is possible to construct an optimized random sampling pattern by drawing indices from a pdf that is generated by using  $k$ -space data as a reference. These data sets can be reconstructed by using the concept of regularized nonlinear inversion for parallel imaging. Due to the fact that the randomized trajectories maximize the incoherence of the aliasing artifacts, their elimination during the reconstruction process is improved. As it is also ensured that an optimal ratio of low to high frequency points is sampled, this allows the use of high acceleration factors while yielding images with considerably reduced artifacts.

## II. THEORY

### A. Optimized random sampling pattern

The design of an optimal sampling pattern (for a given acceleration factor) must take into account two different objectives: the  $k$ -space samples must contain as much information about the sampled image as possible, and the inevitable subsampling artifacts in the reconstruction should be as small as possible. (These are complementary, but not identical, aims, as we will show below.) We propose a way of constructing sampling patterns which fulfill both goals.

The first objective can be expressed in terms of the  $L^2$ -error between the measured data and the true image as follows. Consider the sampling operator  $K\mathcal{F}$  acting on the true image  $u$ , where  $\mathcal{F}$  is the Fourier transform and  $K$  is a mask zeroing out not acquired frequencies. If  $g$  are the measured noisy and subsampled  $k$ -space data and  $\hat{u} = \mathcal{F}u$ , we have

$$\begin{aligned} \|\hat{u} - g\|^2 &= \|K(\hat{u} - g)\|^2 + \|(I - K)(\hat{u} - g)\|^2 \\ &\leq \delta + \|(I - K)\hat{u}\|^2, \quad (1) \end{aligned}$$

This work was supported by the Austrian Science Fund (FWF) under grant SFB F32 (SFB "Mathematical Optimization and Applications in Biomedical Sciences").

\*F. Knoll is with the Institute of Medical Engineering, Graz University of Technology, Kronesgasse 5, A-8010 Graz, Austria, (email: florian.knoll@tugraz.at)

C. Clason is with the Institute for Mathematics and Scientific Computing, University of Graz, Heinrichstrasse 36, A-8010 Graz, Austria, (email: christian.clason@uni-graz.at).

C. Diwoky is with the Institute of Medical Engineering, Graz University of Technology, Kronesgasse 5, A-8010 Graz, Austria, (email: clemens.diwoky@tugraz.at)

R. Stollberger is with the Institute of Medical Engineering, Graz University of Technology, Kronesgasse 5, A-8010 Graz, Austria, (email: rudolf.stollberger@tugraz.at)

where  $\delta$  is the noise level,  $I$  is the identity, and the second term is the sum of the squared magnitude of the not sampled frequencies. This shows that (as intuitively suggested), one should acquire predominantly those coefficients of the image which have the largest magnitude. Of course, this is one of the reasons for the good performance of radial trajectories: Central frequencies, where the energy of images is concentrated, are sampled more densely than the outlying frequencies. However, the linear radial decay of the sampling point density does not sufficiently reflect the true energy distribution of medical images, which does not obey a simple power law (cf. Figure 1).

On the other hand, even if the exact energy density were available, just sampling the highest magnitude coefficients would effectively result in a low pass filter and hence lead to unacceptable loss of resolution (contradicting the goal of minimizing subsampling artifacts). We therefore propose to use a pattern of randomly distributed sampling points, where frequencies corresponding to large coefficients in a template image have a higher probability of being sampled. Such a template can be generated from a pre-scan of a single slice, since the variation arising from randomness of the sampling is greater than the effects of differing energy distributions within the volume (cf. Figure 1). (Of course, such a pre-scan can be used to obtain an estimate of the coil sensitivities as well.) If this is not feasible, it is our observation that a template taken from any reasonably similar medical image will give good results. Indeed, the work in Ref. [7] suggests that a random  $k$ -space distribution will be suitable (even if not optimal) for a large variety of objects. Similarly, as the coil sensitivities have rapidly decaying Fourier coefficients due to their smoothness, these modulations will have minimal impact on the power spectrum outside of the central frequencies. Since the spectrum of the template has its peak at these frequencies as well, the corresponding sampling pattern will almost certainly fully sample these frequencies and thus capture the influence of the modulations sufficiently well.

This suggests the following procedure: Given a reference or template image, we take the magnitude of its Fourier transform, scaled such that the integral is one. This function then serves as a probability density function for the coordinates of a sample point on a fixed uniform Cartesian grid in  $k$ -space, defined by the desired resolution. Using a Monte Carlo method, we draw sampling points until the prescribed acceleration factor is reached. These are then used as the mask  $K$  to construct the nonuniform sampling pattern. This procedure is illustrated in Figure 2. As described in Ref. [3], these randomized sampling trajectories can be easily implemented on MRI-Scanners by using 3D Cartesian encoding. The use of two phase encoding directions gives complete freedom to choose any sample point in the 2D phase encode plane (usually called the  $k_y - k_z$  plane, with  $k_x$  being the direction of frequency encoding).

### B. Nonlinear inversion

The sampling method described above has the added benefit that the subsampling artifacts are incoherent and noise-like, and are thus more amenable to removal during reconstruction, which is our second goal.

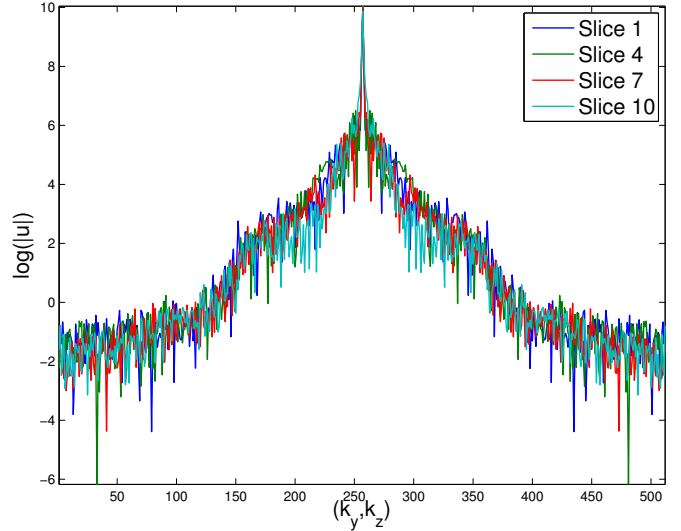


Fig. 1. Logarithm of absolute value of Fourier coefficients of 4 different slices of a  $T_2$  weighted brain scan (two of the slices are displayed in Figure 4 left, middle). The values along a diagonal in  $k$ -space are shown.

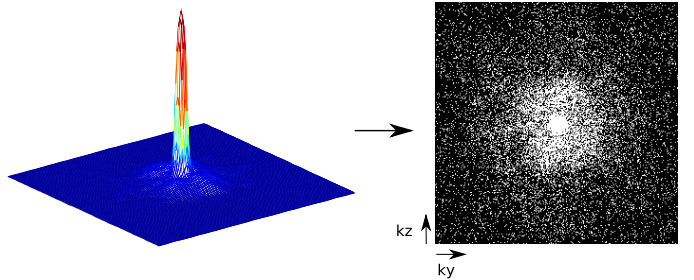


Fig. 2. Example of a pdf (left) and a sampling pattern with subsampling factor  $R = 4$  generated from it using a Monte Carlo method (right).  $k_y$  and  $k_z$  denote the two phase encoding directions; the frequency encoding direction is orthogonal to the image plane. The pdf was obtained from a reference scan and was used to generate the sampling patterns for the in vivo experiments (cf. Figure 8).

This can be quantified using the sidelobe-to-peak ratio of the point spread function (psf) of the sampling operator (cf. Figure 3), which behaves like additive Gaussian noise with zero mean and variance

$$\sigma = \sqrt{\frac{1}{S} - \frac{1}{N^2}}, \quad (2)$$

where  $N$  is the resolution of the image and  $S$  is the number of acquired frequencies per slice [3].

Hence we can model the subsampling errors in the reconstruction from measurements  $g$  using an additive white noise model  $E$ :

$$\mathcal{F}^{-1}g = \mathcal{F}^{-1}K\mathcal{F}u \approx u + E. \quad (3)$$

(Assuming for the moment that the coil sensitivities are known exactly, and we can thus recover the unmodulated image given a modulated  $u$ .) Given no prior estimate on the image (i.e., assuming the pixel values to be random), the maximum a posteriori estimator can be computed as (cf. [10])

$$\arg \min_u \frac{1}{2} \|u - \mathcal{F}^{-1}g\|^2 + \frac{\alpha}{2} \|u\|^2, \quad (4)$$

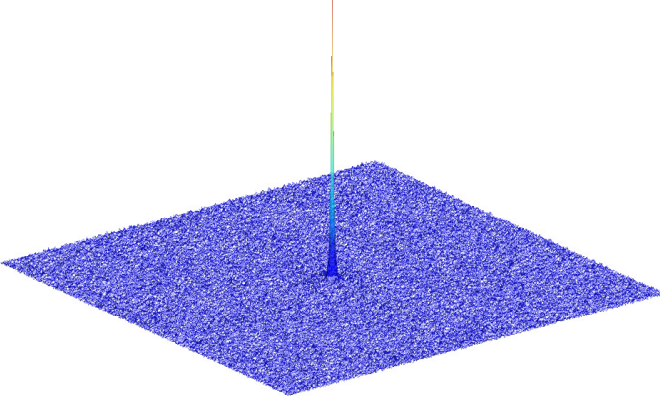


Fig. 3. Example of a psf of random subsampling according to a sampling pattern with subsampling factor  $R \approx 18$  generated from a reference scan (cf. Figure 4, middle).

or equivalently, since the Fourier transform is orthogonal,

$$\arg \min_u \frac{1}{2} \|\mathcal{F}u - g\|^2 + \frac{\alpha}{2} \|\mathcal{F}u\|^2. \quad (5)$$

However, it was shown in Refs. [5], [6], that a joint iterative reconstruction of image and coil sensitivities yields significantly better reconstruction. Of course, any prior information on the sensitivities can be included as an initial guess.

We thus pose the reconstruction problem as solving a nonlinear operator equation  $F(x) = g$ , where  $x := (u, c_1, \dots, c_N)$ ,

$$F : x \mapsto (K\mathcal{F}(u \cdot c_1), \dots, K\mathcal{F}(u \cdot c_N))^T, \quad (6)$$

maps the (pixel-valued) true (unmodulated) image  $u$  and the sensitivities  $c_1, \dots, c_N$  of the  $N$  receiver coils to the set of acquired  $k$ -space coefficients  $g = (g_1, \dots, g_N)^T$  of each coil. Here,  $\cdot$  denotes pointwise multiplication in image space and  $K\mathcal{F}$  is the sampling operator determined by the chosen trajectory. This nonlinear equation can be solved by an iteratively regularized Gauß-Newton (IRGN) method [11], [12], [13], [14], i.e., computing in each step  $k$  the minimum  $\delta x$  of

$$\frac{1}{2} \|F'(x^k)\delta x + F(x^k) - g\|^2 + \frac{\alpha_k}{2} \|W(x^k + \delta x - x^0)\|^2 \quad (7)$$

for given  $\alpha_k > 0$  and an initial guess  $x^0$ , and then setting  $x^{k+1} := x^k + \delta x$ ,  $\alpha_{k+1} := q\alpha_k$  with  $0 < q < 1$ . Here,  $F'(x^k)$  is the Jacobian of  $F$  evaluated at  $x^k$ , and  $W$  is a penalty discussed in section II-C. This procedure can be seen as a nonlinear variant of the Tikhonov regularization (5). Due to the bilinear structure of  $F$ , the action of  $F'(x^k)$  (and its adjoint) can be calculated explicitly using the fast Fourier transform (FFT) (and its inverse), so that the corresponding normal equations can be efficiently solved with a conjugate gradient (CG) method.

If we can assume that the aliasing artifacts dominate the noise, relation (2) allows us to use the discrepancy principle to choose the optimal stopping criterion: Terminate at the first iteration  $k^*$  that satisfies

$$\|F(x^k) - g\| \leq \tau \sqrt{S} \sigma \quad (8)$$

for a fixed  $\tau > 1$ .

### C. Regularization

For the IRGN method to yield good results, proper regularization is critical. As can be seen in equation (6), the same change in the value of  $F$  can be achieved by multiplying  $u$  with some function  $f$  and by dividing all  $c_i$  by  $f$ . Therefore, a priori information must be incorporated to distinguish between necessary updates of  $u$  and  $c_i$ . A generally satisfied assumption is that the sensitivities are very smooth, while the image component can have strong jumps in intensity. This suggests penalizing high frequency oscillations in the form of a weight on the corresponding Fourier coefficients in the  $L^2$ -norm of  $c_i$ . Since the error in the image component  $u$  is assumed to be Gaussian with zero mean, the Fourier coefficients are uniformly weighted, which is equivalent to a standard  $L^2$ -penalty on  $u^k$ . The operator  $W$  in (7) is then expressed as

$$Wx = (\mathcal{F}u, w\mathcal{F}c_1, \dots, w\mathcal{F}c_N)^T, \quad (9)$$

for a suitable weight  $w$  (given below, cf. (16)) which is a monotonically increasing polynomial of  $k_y, k_z$  (assuming the origin of  $k$ -space is in the center).

However, applying  $W$  in every CG iteration is a very ill-conditioned operation, since the weight strongly amplifies the high frequency components and thus the noise inherent in them. It is therefore crucial for the numerical stability of the method to replace  $x$  with  $Wx$  and  $F$  by  $FW^{-1}$  as the independent variable, adapting the derivatives accordingly. In this way, instead of applying a ‘‘coarsening’’ operator (which is ill-posed) in every step, we apply a smoothing operator. In principle, inverting a smoothing operator is equivalent to applying a coarsening operator, but terminating the inner CG method for the solution of the normal equations after a finite number of steps acts as a regularization method.

The application of the IRGN method therefore consists in solving the normal equations for the accordingly modified (7),

$$\begin{aligned} & ((FW^{-1})'(x^k))^H (FW^{-1})'(x^k) + \alpha_k I \delta x = \\ & (FW^{-1})'(x^k)^H ((FW^{-1})(x^k) - g) + \alpha_k (x^0 - x^k), \end{aligned} \quad (10)$$

for  $\delta x = (\delta u, \delta c_1, \dots, \delta c_N)^T$  given  $x^k = (u, c_1, \dots, c_N)^T$  using the CG method.

With  $\bar{z}$  denoting the complex conjugate of the vector  $z$  and  $A^H$  the conjugate transpose of the matrix  $A$ , we set for  $i = 1, \dots, N$

$$W^{-1}c_i = \mathcal{F}^{-1}(w \cdot c_i), \quad (11)$$

$$W^{-H}g_i := (W^{-1})^H g_i = \bar{w} \cdot \mathcal{F}(g_i), \quad (12)$$

where  $w$  has been defined in (16), and obtain

$$\begin{aligned} (FW^{-1})(x^k) = & (K\mathcal{F}(u \cdot W^{-1}c_1), \dots, \\ & K\mathcal{F}(u \cdot W^{-1}c_N))^T. \end{aligned} \quad (13)$$

The derivative acting on the increment  $\delta x$  is then given as

$$(FW^{-1})'(x_k)\delta x = (K\mathcal{F}(u \cdot W^{-1}\delta c_1 + W^{-1}c_1 \cdot \delta u), \dots, K\mathcal{F}(u \cdot W^{-1}\delta c_N + W^{-1}c_N \cdot \delta u))^T, \quad (14)$$

and the adjoint (Hermitian) of the derivative acting on  $\delta g = (\delta g_1, \dots, \delta g_N)$  as

$$(FW^{-1})'(x_k)^H \delta g = \left( \sum_{i=1}^N \overline{W^{-H}c_i} \cdot \mathcal{F}^{-1}\delta g_i, W^{-H}(\bar{u} \cdot \mathcal{F}^{-1}\delta g_1), \dots, W^{-H}(\bar{u} \cdot \mathcal{F}^{-1}\delta g_N) \right)^T. \quad (15)$$

Here, we need not include the sampling mask  $K$  in the definition, since the inputs (i.e., the residual and the derivative) will automatically be subsampled such that the correct entries are zero.

Implementing the CG iterations is now straightforward, requiring only pointwise multiplications and fast Fourier transforms.

### III. METHODS

#### A. Downsampling experiments

As a first proof of principle, a fully sampled  $T_2$  weighted Turbo Spin Echo Scan of the brain of a Multiple Sclerosis (MS) patient was acquired on a clinical 1.5T scanner. This data set was an interesting test for our method because it was possible to assess if the clinically important MS lesions can be distinguished from incoherent aliasing artifacts. Sequence parameters were repetition time  $TR=3845$ ms, echo time  $TE=80$ ms, flip angle  $FA=90^\circ$ , turbo factor 13, 2 signal averages, Matrix Size  $(x,y,z)=512 \times 512$ , 24 slices with a slice thickness of 5mm and an in plane resolution of  $0.44\text{mm} \times 0.44\text{mm}$ . The data set was exported and subsampled retrospectively, to simulate an accelerated acquisition.

Two different downsampling experiments were conducted. In the first experiment, the sampling pattern was constructed by drawing samples from a pdf that was generated with the use of a different slice from the same data set. This corresponds to the situation where a reference scan, prior to the accelerated scan, is used to generate a tailored sampling trajectory individually for each patient.

In the second experiment, the pdf used to generate the sampling pattern was created using a single slice from a frontal scan of the carotid arteries of a different patient. The goal of this experiment was to show that as the power spectra of medical images are very similar, excellent results can be obtained with sampling patterns that are created from scans with completely different properties. Two slices of the  $T_2$  weighted MS data set and the angiography template are displayed in Figure 4.

Subsampling with reduction factors  $R=4$ ,  $R=10$  and  $R=18$  was simulated. It should be noted that as the sampling patterns are generated by a random process, exact values for subsampling factors usually show a slight difference between subsequent runs. Additionally, it might be possible that one particular sampling pattern shows suboptimal performance.

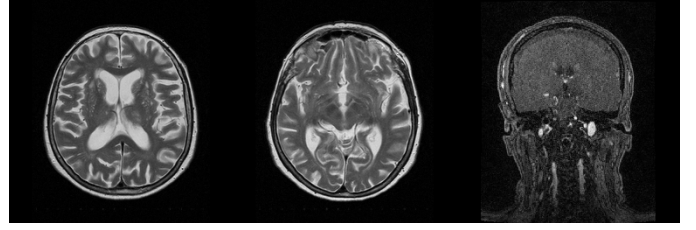


Fig. 4. Left:  $T_2$  weighted brain image that was subsampled and reconstructed. Middle: Different slice from the same  $T_2$  weighted brain data set that served as a template to generate the sampling pdf. Right: Angiography scan that served as a template to generate the sampling pdf.

To guard against this, we repeat the generation of sampling patterns several times, and choose the pattern with the largest incoherence (which can be measured via its Fourier transform, cf. [3]).

Image acquisition with a 4 channel coil array was simulated by modulating the images with coil sensitivities that were generated with the use of Biot-Savart's law.

#### B. MRI data acquisition for phantom and in vivo experiments

MRI data was acquired with a 3D gradient echo sequence. All measurements were conducted at 3T (Siemens Magnetom TIM Trio, Erlangen, Germany). A receive-only 12 channel head coil in triple mode was used, which yields 12 channels with different combinations of the coils. The MRI sequence was modified by including a binary 2D mask that defined the randomized 3D subsampled pattern. The following sequence parameters were used: repetition time  $TR=20$ ms, echo time  $TE=5$ ms, flip angle  $FA=18^\circ$ , matrix size  $(x,y,z)=256 \times 256 \times 256$ . Subsampling with reduction factors  $R=4$ ,  $R=10$  and  $R=18$  was performed. Phantom and brain images of healthy volunteers were acquired. For the phantom experiments, an in plane resolution of  $1\text{mm} \times 1\text{mm}$  and a slice thickness of 5mm was used. The in vivo measurements were obtained with an isotropic spatial resolution of 1mm. Written informed consent was obtained from all volunteers prior to the examination.

The sampling patterns were generated in the following way. Prior to accelerated measurements, a fully sampled single slice was scanned with the same sequence parameters. This scan served as a reference to construct the pdf that was then used to obtain an optimized sampling pattern. For the in vivo measurements a different approach was used additionally to show the generalization potential of the method. In this experiment, a lower resolution reference scan (matrix size  $(x,y,z)=128 \times 128$ ) obtained from a different volunteer several days before the accelerated measurements was used as a template to generate the sampling pattern.

Raw data was exported from the scanner, a 1D Fourier transform was performed along the readout direction, and partitions orthogonal to this axis were reconstructed offline using the described nonlinear inversion method.

#### C. Nonlinear inversion

The IRGN method described above was implemented in Matlab. The weight for the Fourier coefficients of the coil

sensitivities was chosen such that

$$(w \cdot c_i)(k_y, k_z) = (1 + 220(k_y^2 + k_z^2))^{-l} c_i(k_y, k_z) \quad (16)$$

for  $l = 8$ , based on the observed spectrum of sensitivities generated according to Biot-Savart's law.

All parameters were chosen dependent on the measured data  $g$ , which for reasons of comparability was scaled to have norm  $\|g\| = 100$ . The initial regularization parameter  $\alpha_0$  was chosen such that the norm of the residual in step 1 satisfies

$$\|F(x^1) - g\| \approx \frac{3}{4} \|F(x^0) - g\|, \quad (17)$$

and the reduction factor  $q$  such that in further iterations  $k$ ,

$$\|F(x^{k+1}) - g\| \approx \frac{1}{3} \|F(x^k) - g\| \quad (18)$$

holds. In the experiments described here, this yielded  $\alpha_0 = 1$  and  $q = 0.1$ . The linear system in each iteration was solved using the method of conjugate gradient, which was stopped if an iteration-dependent relative tolerance  $\epsilon_k := \frac{1}{3} \alpha_k$  was reached (cf. [15]). The IRGN iteration was stopped according to the discrepancy principle (8) with  $\tau = 2.2$ . Of course, it is impossible to guarantee in practice that the assumption of the reconstruction errors dominating the noise will be satisfied, and thus that the stopping criterion can be attained. Since the proposed method also has to be applicable in cases where this assumption does not hold, we imposed an additional heuristic, but robust and data-independent, stopping criterion of L-curve type: After a fixed maximum number of iterations (10 in our case) was reached, we chose the last iterate for which the residual norm was noticeably decreased, i.e.,

$$\|F(x^k) - g\| < \frac{3}{4} \|F(x^{k-1}) - g\|. \quad (19)$$

Finally, we multiply the reconstructed image  $u^*$  by the square root of the sum of squares of the reconstructed sensitivities:

$$u = u^* \cdot \sqrt{\sum_{i=1}^N |c_i^*|^2}. \quad (20)$$

Although it is not crucial for the convergence of the algorithm, this post-processing step can improve the quality of the reconstruction by removing residual smooth modulations in the image and serving as a mask to remove residual noise in regions where the image is zero.

For comparison, images were also reconstructed with a conventional inverse Fourier transform with density compensation corresponding to the nonuniform sampling pattern, followed by a sum of squares (SOS) combination of the individual coil images  $\mathcal{F}^{-1}g_1, \dots, \mathcal{F}^{-1}g_N$ .

## IV. RESULTS

### A. Downsampling experiments

The results of the downsampling experiments are depicted in Figures 5 and 6. It is not surprising that incoherent undersampling artifacts showing noise-like characteristics appear in conventional SOS reconstructions. However, it should be noted that due to the proposed method of generating the

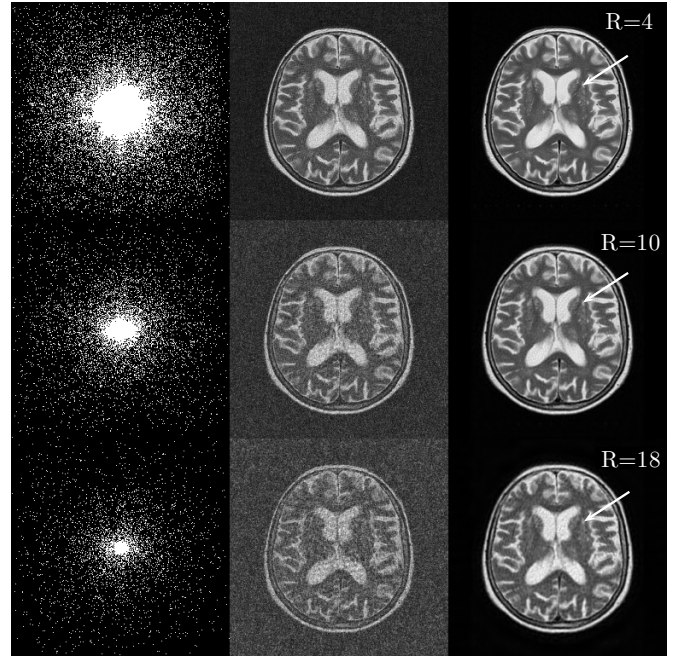


Fig. 5. Downsampling experiment reconstruction results for different subsampling factors  $R$ . A different slice from the  $T_2$  weighted brain scan was used as a template to generate the sampling trajectory (see Figure 4). Left column: Used sampling pattern. Middle column: Conventional SOS combination of the individual coil images. Right column: IRGN reconstruction. Top row:  $R=4$ . Middle row:  $R=10$ . Bottom row:  $R=18$ . MS lesions (indicated by arrows) which are completely buried below incoherent aliasing in the SOS reconstructions can still be identified in the IRGN reconstructions.

sampling pattern, fair image quality can be obtained with a SOS reconstruction for an undersampling factor of 4 in both experiments.

Excellent image quality can be achieved with the IRGN method for  $R=4$  and  $R=10$ . Undersampling artifacts are removed efficiently, the images show high SNR, and fine details are preserved. In particular, MS lesions can still be identified which are buried below artifacts in the SOS reconstructions. In contrast, in the experiment with  $R=18$ , residual artifact remain visible in the IRGN reconstruction. The results of the experiments with the reference scan and the angio template are comparable which illustrates the generalization potential of the method.

### B. Phantom measurements

The results from the downsampling experiments are confirmed in the phantom studies. Figure 7 depicts the results for acceleration factors  $R=4$ ,  $R=10$  and  $R=18$ . IRGN results show excellent image quality and good SNR, even in the extreme case of  $R = 18$  when the acceleration factor was higher than the number of receiver coils. Again, it is worth noting that for  $R=4$ , image quality is surprisingly high in the conventional sum of squares reconstruction due to the optimized sampling pattern.

### C. In vivo measurements

Figure 8 shows the results of the experiment where the low resolution template scan of a different volunteer several days

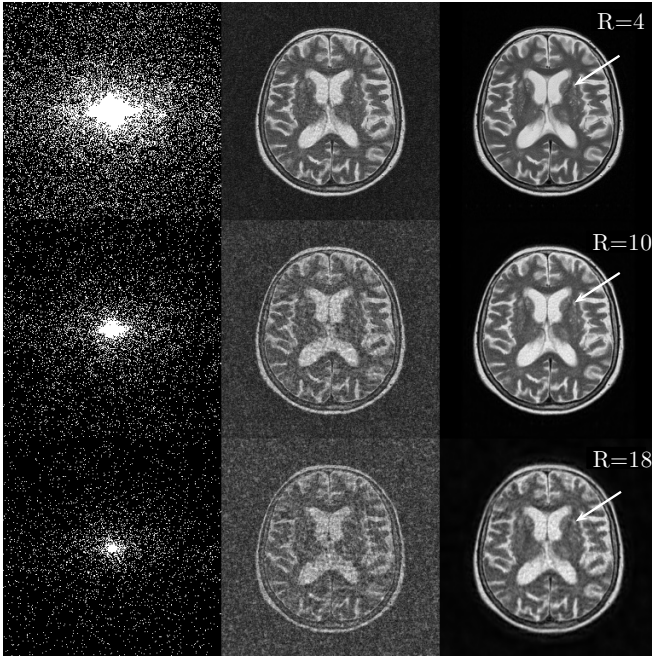


Fig. 6. Downsampling experiment reconstruction results for different subsampling factors  $R$ . The angiography scan from Figure 4 was used as a template to generate the sampling trajectory. Left column: Used sampling pattern. Middle column: Conventional SOS combination of the individual coil images. Right column: IRGN reconstruction. Top row:  $R=4$ . Middle row:  $R=10$ . Bottom row:  $R=18$ . MS lesions (indicated by arrows) which are completely buried below incoherent aliasing in the SOS reconstructions can still be identified in the IRGN reconstructions.

before the accelerated measurements was used to generate the sampling pattern. IRGN results with  $R=4$  and  $R=10$  show excellent removal of aliasing artifacts, high SNR and no loss of fine image details. The reconstruction from the  $R=18$  data set is already deteriorated by noise, but it should be noted that this is an extremely challenging situation for the reconstruction algorithm, as the acceleration factor is higher than the number of receiver coils and SNR is quite low due to the isotropic voxel volume of  $1\text{mm}^3$ .

The results for the experiment where a conventional reference scan was obtained prior to subsampled measurements are displayed in Figure 9. Image quality of all acceleration factors is comparable to the reconstructions in Figure 8. This supports the hypothesis that it is possible to generate sampling patterns with good generalization potential for a wider range of scans.

## V. DISCUSSION

An optimized random sampling pattern for 3D parallel imaging is presented. The method allows generating tailored sampling patterns for each individual patient by making use of a pre-scan. As this is often already done in the context of parallel imaging to estimate the sensitivities, a pre-scan will take no additional time in this case. If this is not feasible, it was shown that the generalization potential of the method is high enough to ensure that excellent results can be achieved with precomputed sampling patterns that were generated from template scans. With the proposed method, excellent removal

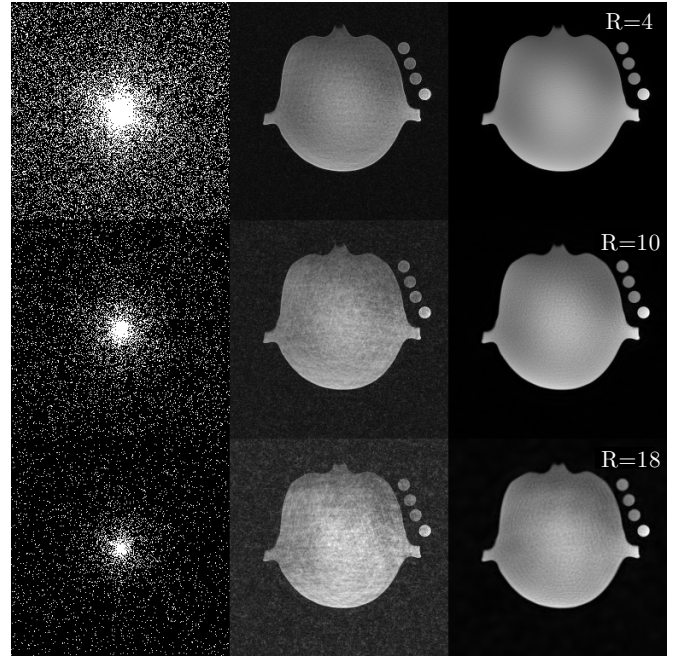


Fig. 7. Results of phantom measurements for different subsampling factors  $R$ . A reference scan was performed to generate the sampling pattern. Left column: Used sampling pattern. Middle column: Conventional sum of squares combination of the individual coil images. Right column: IRGN reconstruction. Top row:  $R=4$ . Middle row:  $R=10$ . Bottom row:  $R=18$

of undersampling artifacts was achieved for high acceleration factors while fine image details were preserved.

In principle, the method could be used with any type of parallel imaging, but using the nonlinear inversion methods ensures that better estimates of the coil sensitivities are obtained during the reconstruction process. This leads to an additional improvement in reconstruction quality. Of course it would also be possible to use the proposed acquisition patterns to improve the reconstruction quality in methods based on compressed sensing.

A software package is provided which allows reproducing some of the results described in this paper. It can be downloaded from [http://math.uni-graz.at/mobis/software/irgn\\_random.zip](http://math.uni-graz.at/mobis/software/irgn_random.zip).

### A. Choice of parameters

In all our tests, the method proved to be quite robust with respect to the parameters, with the obvious exception of the stopping criterion (see below). The reduction parameters  $\alpha_0$  and  $q$  effectively only determined the number of iterations necessary to reach a certain residual norm (the larger the parameters, the more iterations were needed), and the computation time (since the tolerance in the CG method is coupled to  $\alpha_k$ ). This is due to the bilinear structure of the problem, which means that for fixed  $\alpha$  and a good initial guess, the (non-iteratively regularized) Gauß-Newton method would converge in very few steps. The final iterates are therefore mainly determined by the current value of  $\alpha$ , and little by the previous iterations.

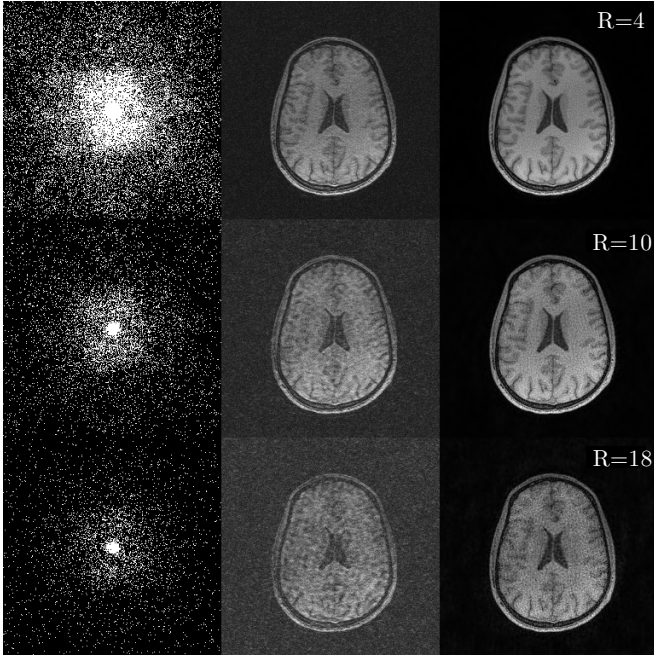


Fig. 8. Results of in vivo measurements for different subsampling factors  $R$ . A low resolution scan of a different volunteer was performed to generate the sampling pattern. Left column: Used sampling pattern. Middle column: Conventional sum of squares combination of the individual coil images. Right column: IRGN reconstruction. Top row:  $R=4$ . Middle row:  $R=10$ . Bottom row:  $R=18$

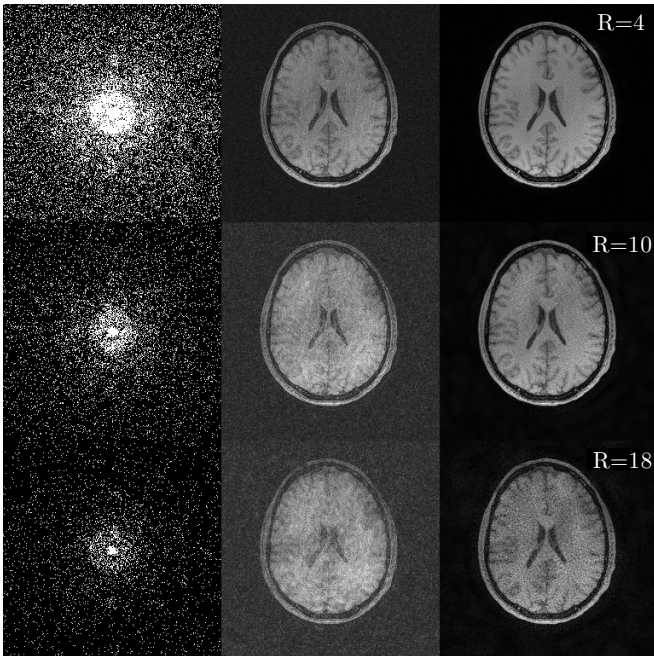


Fig. 9. Results of in vivo measurements for different subsampling factors  $R$ . A reference scan was performed to generate the sampling pattern. Left column: Used sampling pattern. Middle column: Conventional sum of squares combination of the individual coil images. Right column: IRGN reconstruction. Top row:  $R=4$ . Middle row:  $R=10$ . Bottom row:  $R=18$

Similarly, the parameter  $l$  only played a noticeable role for the first few iterations, after which the penalty parameter was small enough to allow large changes in the sensitivity components even for high smoothness penalties.

### B. Convergence and stopping criterion

The outer Gauß-Newton iteration terminated in almost all cases after around 5 steps, at which point the stopping criterion (8) was satisfied. For the in vivo measurements with acceleration factor of  $R = 4$ , due the combination of low aliasing error and low SNR, the iteration was terminated by the secondary criterion (19) after the residual norm has been reduced below 6% of the initial residual, which coincided with the point where noise amplification started to occur. Again, this amounted to about 5 iterations for each slice.

The convergence of the inner CG iterations depended on the outer iteration via the iterative reduction of the tolerance. Typically, in all but the last few iterations, the tolerance was achieved; in the other cases (the tolerance being below  $10^{-6}$ ) the maximum number of iterations was reached with a residual norm below  $10^{-4}$ , which is sufficient for purposes of image reconstruction.

### C. Computational speed

Due to the data dependent choice of parameters, the number of iterations necessary is fairly independent of the data size. That means that the running time scales linearly with respect to the number of coils and slices, and quadratically with respect to the image size, while being constant in the reduction factor. The decrease in acquisition time is therefore not offset by an increase in reconstruction time.

Specifically, our proof-of-concept implementation in Matlab on a 2.4 GHz workstation (using a single core) needed around 110 seconds for a single slice of the downsampling experiments (size  $512 \times 512$ , four coils), and between 80 and 160 seconds (depending on the number of iterations) for one in vivo slice (size  $256 \times 256$ , 12 coils). While this is no significant problem in research applications, it is still too slow for daily clinical practice. But as the algorithm is essentially FFT-dominated, it is expected that a native implementation on graphics hardware (e.g., using CUDA [16]) will increase the performance by at least two orders of magnitude.

## VI. CONCLUSIONS

This work presents a new method for highly accelerated parallel imaging. The method is easy to implement and can be integrated in any 3D Cartesian pulse sequence. As Cartesian encoding is used in the vast majority of scans in daily clinical practice, it is expected that numerous applications can benefit from the prospect of highly reduced scan time. Examples that will be studied during future work include iron mapping in the brain, angiography and perfusion imaging.

## ACKNOWLEDGMENTS

The authors thank Martin Uecker for helpful discussions about the IRGN method, and Prof. Franz Fazekas for his help with the MS patient data.

## REFERENCES

- [1] K. P. Pruessmann, M. Weiger, M. B. Scheidegger, and P. Boesiger, "SENSE: sensitivity encoding for fast MRI." *Magn Reson Med*, vol. 42, no. 5, pp. 952–962, Nov 1999.
- [2] M. A. Griswold, P. M. Jakob, R. M. Heidemann, M. Nittka, V. Jellus, J. Wang, B. Kiefer, and A. Haase, "Generalized autocalibrating partially parallel acquisitions (GRAPPA)." *Magn Reson Med*, vol. 47, no. 6, pp. 1202–1210, Jun 2002.
- [3] M. Lustig, D. Donoho, and J. M. Pauly, "Sparse MRI: The application of compressed sensing for rapid MR imaging." *Magn Reson Med*, vol. 58, no. 6, pp. 1182–1195, Dec 2007.
- [4] K. T. Block, M. Uecker, and J. Frahm, "Undersampled radial MRI with multiple coils. iterative image reconstruction using a total variation constraint." *Magn Reson Med*, vol. 57, no. 6, pp. 1086–1098, Jun 2007.
- [5] M. Uecker, T. Hohage, K. T. Block, and J. Frahm, "Image reconstruction by regularized nonlinear inversion—joint estimation of coil sensitivities and image content." *Magn Reson Med*, vol. 60, no. 3, pp. 674–682, Sep 2008.
- [6] F. Knoll, C. Clason, M. Uecker, and R. Stollberger, "Improved reconstruction in non-cartesian parallel imaging by regularized nonlinear inversion," in *Proceedings of the 17th Scientific Meeting and Exhibition of ISMRM, Honolulu, HI, 2009*.
- [7] Marseille, de Beer R, Fuderer, Mehlkopf, and van Ormondt D, "Nonuniform phase-encode distributions for MRI scan time reduction," *J Magn Reson B*, vol. 111, no. 1, pp. 70–75, Apr 1996.
- [8] C. M. Tsai and D. G. Nishimura, "Reduced aliasing artifacts using variable-density k-space sampling trajectories." *Magn Reson Med*, vol. 43, no. 3, pp. 452–458, Mar 2000.
- [9] A. Greiser and M. von Kienlin, "Efficient k-space sampling by density-weighted phase-encoding." *Magn Reson Med*, vol. 50, no. 6, pp. 1266–1275, Dec 2003.
- [10] J. Kaipio and E. Somersalo, *Statistical and computational inverse problems*, ser. Applied Mathematical Sciences. New York: Springer-Verlag, 2005, vol. 160.
- [11] A. B. Bakushinsky and M. Y. Kokurin, *Iterative methods for approximate solution of inverse problems*, ser. Mathematics and Its Applications (New York). Dordrecht: Springer, 2004, vol. 577.
- [12] H. W. Engl, M. Hanke, and A. Neubauer, *Regularization of inverse problems*, ser. Mathematics and its Applications. Dordrecht: Kluwer Academic Publishers Group, 1996, vol. 375.
- [13] B. Blaschke, A. Neubauer, and O. Scherzer, "On convergence rates for the iteratively regularized Gauss-Newton method," *IMA J. Numer. Anal.*, vol. 17, no. 3, pp. 421–436, 1997.
- [14] T. Hohage, "Logarithmic convergence rates of the iteratively regularized Gauss-Newton method for an inverse potential and an inverse scattering problem," *Inverse Problems*, vol. 13, no. 5, pp. 1279–1299, 1997.
- [15] ———, "On the numerical solution of a three-dimensional inverse medium scattering problem," *Inverse Problems*, vol. 17, no. 6, pp. 1743–1763, 2001.
- [16] NVIDIA, *NVIDIA CUDA Programming Guide 2.0*. NVIDIA Cooperation, 2008.